



AALBORG UNIVERSITY
DENMARK

Aalborg Universitet

Generation of robust bispecific antibodies through fusion of single-domain antibodies on IgG scaffolds: a comprehensive comparison of formats

Madsen, Andreas V.; Kristensen, Peter; Buell, Alexander K.; Goletz, Steffen

Published in:
mAbs

DOI (link to publication from Publisher):
[10.1080/19420862.2023.2189432](https://doi.org/10.1080/19420862.2023.2189432)

Creative Commons License
CC BY-NC 4.0

Publication date:
2023

Document Version
Publisher's PDF, also known as Version of record

[Link to publication from Aalborg University](#)

Citation for published version (APA):

Madsen, A. V., Kristensen, P., Buell, A. K., & Goletz, S. (2023). Generation of robust bispecific antibodies through fusion of single-domain antibodies on IgG scaffolds: a comprehensive comparison of formats. *mAbs*, 15(1), [2189432]. <https://doi.org/10.1080/19420862.2023.2189432>

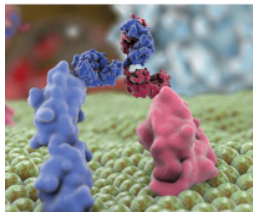
General rights

Copyright and moral rights for the publications made accessible in the public portal are retained by the authors and/or other copyright owners and it is a condition of accessing publications that users recognise and abide by the legal requirements associated with these rights.

- Users may download and print one copy of any publication from the public portal for the purpose of private study or research.
- You may not further distribute the material or use it for any profit-making activity or commercial gain
- You may freely distribute the URL identifying the publication in the public portal -

Take down policy

If you believe that this document breaches copyright please contact us at vbn@aub.aau.dk providing details, and we will remove access to the work immediately and investigate your claim.



Generation of robust bispecific antibodies through fusion of single-domain antibodies on IgG scaffolds: a comprehensive comparison of formats

Andreas V. Madsen, Peter Kristensen, Alexander K. Buell & Steffen Goletz

To cite this article: Andreas V. Madsen, Peter Kristensen, Alexander K. Buell & Steffen Goletz (2023) Generation of robust bispecific antibodies through fusion of single-domain antibodies on IgG scaffolds: a comprehensive comparison of formats, mAbs, 15:1, 2189432, DOI: [10.1080/19420862.2023.2189432](https://doi.org/10.1080/19420862.2023.2189432)

To link to this article: <https://doi.org/10.1080/19420862.2023.2189432>



© 2023 The Author(s). Published with license by Taylor & Francis Group, LLC.



[View supplementary material](#)



Published online: 20 Mar 2023.



[Submit your article to this journal](#)



Article views: 3746



[View related articles](#)



[View Crossmark data](#)

Generation of robust bispecific antibodies through fusion of single-domain antibodies on IgG scaffolds: a comprehensive comparison of formats

Andreas V. Madsen ^a, Peter Kristensen ^b, Alexander K. Buell ^a, and Steffen Goletz ^a

^aDepartment of Biotechnology and Biomedicine, Technical University of Denmark, Kgs. Lyngby, Denmark; ^bDepartment of Chemistry and Bioscience, Aalborg University, Aalborg, Denmark

ABSTRACT

Bispecific antibodies (bsAbs) enable dual binding of different antigens with potential synergistic targeting effects and innovative therapeutic possibilities. The formation of bsAbs is, however, often dependent on complex engineering strategies with a high risk of antibody chain mispairing leading to contamination of the final product with incorrectly assembled antibody species. This study demonstrates formation of bsAbs in a generic and conceptually easy manner through fusion of single-domain antibodies (sdAbs) onto IgG scaffolds through flexible 10 amino acid linkers to form high-quality bsAbs with both binding functionalities intact and minimal product-related impurities. SdAbs are attractive fusion partners due to their small and monomeric nature combined with antigen-binding capabilities comparable to conventional human antibodies. By systematically comparing a comprehensive panel of symmetric αPD-L1×αHER2 antibodies, including reversely mirrored antigen specificities, we investigate how the molecular geometry affects production, stability, antigen binding and CD16a binding. SdAb fusion of the heavy chain was generally preferred over light chain fusion for promoting good expression and high biophysical stability as well as maintaining efficient binding to both antigens. We find that N-terminal sdAb fusion might sterically hinder antigen-binding to the Fv region of the IgG scaffold, whereas C-terminal fusion might disturb antigen-binding to the fused sdAb. Our work demonstrates a toolbox of complementary methods for in-depth analysis of key features, such as in-solution dual antigen binding, thermal stability, and aggregation propensity, to ensure high bsAb quality. These techniques can be executed at high-throughput and/or with very low material consumption and thus represent valuable tools for bsAb screening and development.

ARTICLE HISTORY

Received 6 January 2023
Revised 19 February 2023
Accepted 7 March 2023

KEYWORDS



Antibody; bispecific; flow-induced dispersion analysis; fusion proteins; HER2; IgG-like; PD-L1; single-domain antibody; symmetric


Introduction

Bispecific antibodies (bsAbs) are emerging as a highly promising class of next-generation biotherapeutics. Their ability to simultaneously engage two distinct epitopes is enabling synergistic binding functionalities that cannot be obtained through combinations of conventional monoclonal antibodies.^{1–3} While IgG molecules typically adhere to a Y-shaped molecular architecture, bsAbs can be constructed with a myriad of different molecular geometries from various antibody “building blocks”.⁴ The bsAb format has been found to directly influence antibody functionality,⁵ meaning that similar bsAbs constructed from the exact same molecular building blocks but with different molecular architectures can behave functionally differently. Examples illustrating the importance of spatial arrangements in bsAb dual binding include improved blocking by distinct molecular geometries of biparatopic bsAbs⁶ as well as large differences in natural killer (NK) cell activation for bsAbs with single-chain variable region (scFv) fragments fused C- or N-terminally.⁷ Most clinically developed bsAbs belong to the class of asymmetric antibodies that deviates from the usual paired heavy chain-light chain (HC₂LC₂) symmetry by including more than two antibody chains in the final assembly.⁸ The

asymmetric format is popular because combining different HC and/or LC allows construction of bsAbs with a close resemblance to the native Y-shaped IgG in an attempt to harness the favorable quality attributes of conventional IgG molecules. The complex assembly of asymmetric, heterodimeric bsAbs, however, creates a risk of chain mispairing, which introduces antibody-related impurities that can be difficult to remove because their physicochemical properties tend to closely resemble the desired target heterodimeric bsAb.^{9,10} The issue is typically addressed through advanced engineering of the antibody chains to promote correct polypeptide assembly⁴ or through modifications that allow selective purification of the heterodimeric bsAb product over their undesired homodimeric counterparts.⁹

Another, more straightforward, way for constructing bsAbs is through simple genetic fusion of independent antibody binding domains. Linking of small modular antibody fragments onto larger IgG scaffolds basically expands the binding repertoire of the IgG while retaining the favorable effects from the backbone, namely the Fc effector functions and the prolonged half-life from FcRn recycling. The fusion creates symmetric bsAbs that still adhere to the HC₂LC₂ format, which

CONTACT Steffen Goletz  sgoletz@dtu.dk  Department of Biotechnology and Biomedicine, Technical University of Denmark, Søtofts Plads, Building 224, Kgs Lyngby 2800, Denmark

 Supplemental data for this article can be accessed online at <https://doi.org/10.1080/19420862.2023.2189432>

© 2023 The Author(s). Published with license by Taylor & Francis Group, LLC.

This is an Open Access article distributed under the terms of the Creative Commons Attribution-NonCommercial License (<http://creativecommons.org/licenses/by-nc/4.0/>), which permits unrestricted non-commercial use, distribution, and reproduction in any medium, provided the original work is properly cited. The terms on which this article has been published allow the posting of the Accepted Manuscript in a repository by the author(s) or with their consent.

limits the risk of mispairing that is seen for the asymmetric bsAbs. The positive features of symmetric bsAbs are highlighted by the number of symmetric bsAbs entering into clinical trials.⁸ Selection of a proper molecular architecture is of great importance because the binding domains and their relative orientation to each other might affect the functionality – a hypothesis that has previously been formulated as “format defines function”.¹¹ To date, most fusions of antibody fragments onto IgG scaffolds have been made using scFvs because these fragments are small while often retaining full binding capacity compared to their native Fab. However, scFvs are known to suffer from thermodynamic instability¹² and fusion of scFvs onto IgG scaffolds to form bsAbs has previously been shown to be problematic because of aggregation and improper bsAb assembly.^{13,14} Single-domain antibodies (sdAbs) are the smallest antibody-derived fragments that retain full antigen-binding functionality and they represent an attractive group of fusion partners due to their small size (~15 kDa), high stability, good solubility and monomeric nature.¹⁵

In this work we investigated the formation of symmetric bsAbs through fusion of sdAbs onto IgG1 scaffolds and characterized the effect of the molecular architecture on the biophysical and biochemical properties of these bsAbs. We have previously reported formation of symmetric bsAbs targeting programmed cell death ligand 1 (PD-L1) and human epidermal growth factor receptor 2 (HER2) through fusion of an anti-HER2 (α HER2) sdAb onto an anti-PD-L1 (α PD-L1) IgG1.¹⁶ Here, we expand the molecular repertoire by constructing a comprehensive set of α PD-L1 \times α HER2 bsAbs through fusion of both α HER2 sdAbs onto α PD-L1 IgG1 and fusion of α PD-L1 sdAbs onto α HER2 IgG1. By constructing different bsAbs with the same combination of specificities and molecular geometries, but with the relative position of specificities in the binding domains reversed (Figure 1a) we aimed to assess the effect of the molecular scaffold on bsAb behavior. We find that the molecular format has an effect on both production and functionality of the bsAbs and that many of these observations are consistent across both specificity orientations, thus supporting that the observed effects are rooted in the molecular scaffold. Additionally, our work introduces a toolbox of analytical techniques suited for in-depth characterization of binding activity and drug-like qualities of the increasingly complex bsAbs entering drug development programs.

Results

Design and expression of symmetric anti-PD-L1 \times anti-HER2 bsAbs

In this study, we sought to characterize symmetric IgG-like bsAbs formed through genetic fusion of sdAbs onto full-length IgG1 molecules, extending our previous work.¹⁶ In brief, we constructed bsAbs targeting PD-L1 and HER2 by genetically fusing sdAb fragments onto full-length IgG1 molecules to form symmetric IgG1-like bsAbs. As “building blocks” we used sequences of previously reported α PD-L1 atezolizumab Fv,^{17,18} α HER2 trastuzumab Fv,¹⁹ α PD-L1 KN035 (envalofimab) sdAb²⁰ and α HER2 2Rs15d sdAb.²¹ For the bsAbs we

used a flexible 10-aa GS linker as this type of linker has previously been shown to be effective in linking antibody fragments to IgG1 scaffolds.^{22–24} Fusion of sdAbs onto IgG scaffolds represents a generic and conceptually easy way of forming bsAbs without the need for complex engineering strategies to avoid chain mispairing, which is a common issue in production of bsAbs.⁹ We use a naming scheme denoting the fusion site and the IgG1 scaffold for the specific bsAb, i.e., NHC- α PD-L1 IgG is the anti-PD-L1 IgG1 with α HER2 sdAb fused N-terminally on HC and CLC- α HER2 IgG represent the bsAb where anti-PD-L1 sdAb has been fused C-terminally on the LC of the anti-HER2 IgG1 (Figure 1a).

BsAbs were transiently expressed in HEK293F suspension cells via secretion into the culture supernatant and subsequently purified with one-step Protein A chromatography. The yields after purification were calculated from the purification chromatograms and showed good correlation compared to a biolayer interferometry (BLI) quantitation assay directly on the crude supernatants (Table 1 and Figure S2). The BLI measurements were performed on three replicate cultures from three separate transfections for most of the antibodies and generally showed low variability as indicated by the small standard deviations. The replicate cultures were pooled before purification. Even though many of the bsAbs were constructed from the same molecular building blocks, and hence share the same total amino acid content, notable differences in protein expression yields were observed. Typical yields of the antibodies after purification of supernatants from shake flask cultures were in the range of 40–75 mg/L (Table 1), comparable to previous symmetric bsAb productions.²³ Interestingly, sdAb fusion on the HC (both N-terminally and C-terminally) gave higher expression yields than the parent IgG1, which has also previously been shown for C-terminal HC fusion.²³ Generally, antibody constructs with sdAb fusions on HC seem to produce higher yields compared to the LC-fused constructs.

We used sodium dodecyl sulfate – polyacrylamide gel electrophoresis (SDS-PAGE) and capillary electrophoresis (CE) to verify antibody sizes and assess the purity after Protein A purification. The main impurity appeared to be antibody-related HC dimer without paired LC, which was primarily observed for LC-fused constructs, but not for IgG molecules or tetravalent HC-fused bsAbs (Table 1 and S1). The unpaired HC dimers might point to a change in expression of the engineered LC genes, although further studies would be needed to investigate how sdAb fusion affects the expression levels. Analytical size exclusion chromatography (SEC) showed a low aggregation propensity of the bsAb constructs (0.3%–4.4% of total protein was eluted as higher molecular weight (MW) structures) and dynamic light scattering (DLS) showed good sample homogeneity (low polydispersity index) and estimated hydrodynamic radii in agreement with previously reported sizes of monospecific IgG1 antibodies.²⁵ The low polydispersity of the samples allowed cumulant radius analysis. The cumulant radii generally seemed to follow the theoretical MWs, i.e., IgG1 molecules appeared larger than sdAb-Fc constructs but smaller than the bsAbs, thus demonstrating an expected correlation between MW and size (Figure S3).²⁶ The findings show that the symmetric IgG-like bsAbs

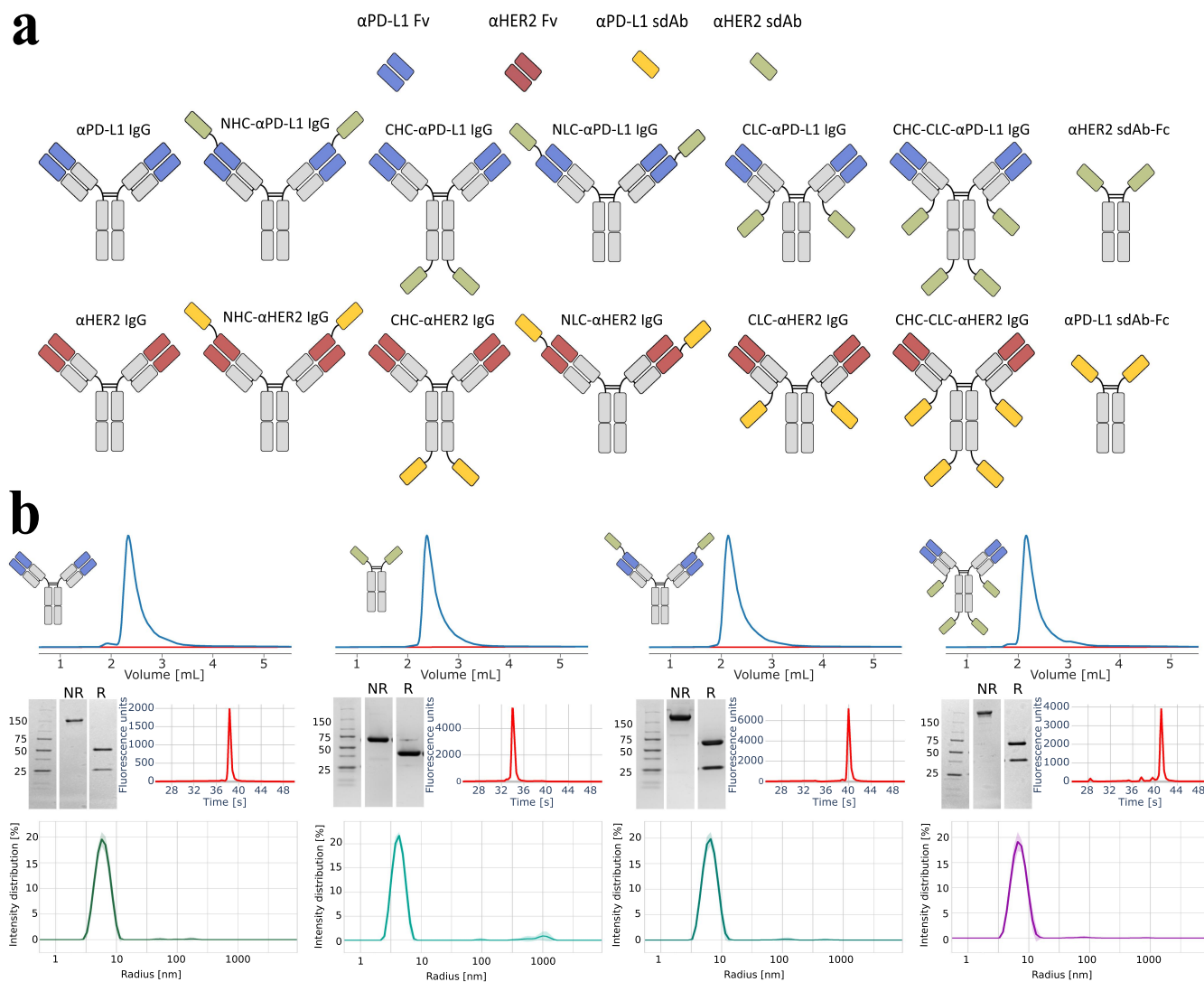


Figure 1. Generation of bispecific αPD-L1xαHER2 antibody formats. (a) Schematic illustration of the bsAbs targeting PD-L1 and HER2 that were generated by fusing αPD-L1 sdAb and αHER2 sdAb onto the αHER2 IgG1 and αPD-L1 IgG1 scaffolds, respectively. The sdAbs were fused both N-terminally and C-terminally on both HC and LC through a flexible (GGGGS)₂ linker. (b) Examples of antibody assembly and sample homogeneity of four representative antibodies. The antibodies were analyzed using analytical size exclusion chromatography (SEC, baseline shown in red; top), SDS-PAGE gel electrophoresis under both reducing (R) - and nonreducing (NR) conditions (middle left), capillary electrophoresis (CE; middle right) and dynamic light scattering (DLS, shown is the intensity weighed size distribution; bottom). Only minute trace amounts of aggregated antibodies can be seen as a tiny left shoulder on the SEC chromatograms as well as larger species in the DLS size distribution plot thereby illustrating high sample homogeneity. Data for the remaining antibodies is available in the supplemental material (S1).

can be robustly produced with high purity and sample homogeneity using a single protein A purification step (Table 1 and Figure 1b).

Biophysical stability tests

In addition to target binding, therapeutic antibodies are typically evaluated with respect to a number of other physicochemical properties that are important for development as drug candidates. Such properties are commonly referred to as a “developability” profile and they have been shown to correlate with successful clinical development.²⁷ We tested the conformational and colloidal stability of our antibody panel to assess any potential effects from the engineering. Thermal unfolding experiments were performed using differential scanning fluorimetry (DSF), which allows simultaneous

monitoring of unfolding and aggregation within the sample to assess the relationship between these factors²⁸ (Figure 2). DSF measures fluorescence emission intensity values at 350 nm and 330 nm after excitation at 280 nm, since protein unfolding events are most often associated with spectral shifts at these wavelengths when tryptophan residues become solvent-exposed during unfolding. The DSF instrument is additionally equipped with optics for DLS and backreflection, which allows aggregation to be monitored in a complementary manner. While DLS is sensitive to the formation of small numbers of aggregates, backreflection is less sensitive and detects only large-scale aggregation of the sample. The thermal unfolding profiles indicate that the sdAb fusion does not cause major changes in structural integrity compared to the parent IgG1 molecules. The bsAbs and parent IgG1 molecules all appeared to undergo two distinct unfolding events, which have been

Table 1. Quality assessment of the produced antibodies.

Antibody	MABSelect Sure yield (mg/L)	BLI quantitation (mg/L)	CE monomer peak (%)	SEC aggregation peak (%)	DLS cumulant radius (nm)	DLS polydispersity index	Calculated MW (kDa)
α PD-L1 IgG	40.8	63.8 \pm 3.6	97.7	2.1	5.63 \pm 0.1	0.12 \pm 0.03	144.6
α PD-L1 sdAb-Fc	53.8	111.0 \pm 2.7	97.0	0.4	4.36 \pm 0.07	0.15 \pm 0.03	78.7
NHC- α PD-L1 IgG	76.4	107.5 \pm 1.9	96.6	0.3	6.23 \pm 0.09	0.09 \pm 0.02	171.1
CHC- α PD-L1 IgG	71.8	96.5 \pm 2.7	97.3	1.1	6.27 \pm 0.09	0.09 \pm 0.02	171.1
NLC- α PD-L1 IgG	17.1	20.3 \pm 0.5	96.5	0.8	6.50 \pm 0.14	0.12 \pm 0.03	171.1
CLC- α PD-L1 IgG	56.0	77.5 \pm 2.6	82.5	2.1	6.26 \pm 0.17	0.14 \pm 0.04	171.1
CHC-CLC- α PD-L1 IgG	75.9	101.5	85.5	1.4	6.82 \pm 0.18	0.07 \pm 0.04	197.6
α HER2 IgG	40.3	57.0 \pm 3.7	92.8	9.2	6.44 \pm 0.47	0.19 \pm 0.16	145.3
α HER2 sdAb-Fc	75.4	124.6 \pm 1.9	97.7	0.4	4.35 \pm 0.18	0.16 \pm 0.11	76.32
NHC- α HER2 IgG	69.8	106.2 \pm 5.5	97.0	0.5	6.57 \pm 0.16	0.15 \pm 0.06	174.2
CHC- α HER2 IgG	72.2	117.5 \pm 2.4	97.4	1.8	6.66 \pm 0.19	0.12 \pm 0.03	174.2
NLC- α HER2 IgG	11.2	14.6 \pm 0.8	61.0	3.1	7.11 \pm 0.08	0.22 \pm 0.02	174.2
CLC- α HER2 IgG	15.4	20.4 \pm 1.6	72.1	4.5	6.32 \pm 0.07	0.12 \pm 0.01	174.2
CHC-CLC- α HER2 IgG	33.3	54.2	69.4	2.9	7.08 \pm 0.04	0.09 \pm 0.02	203.0

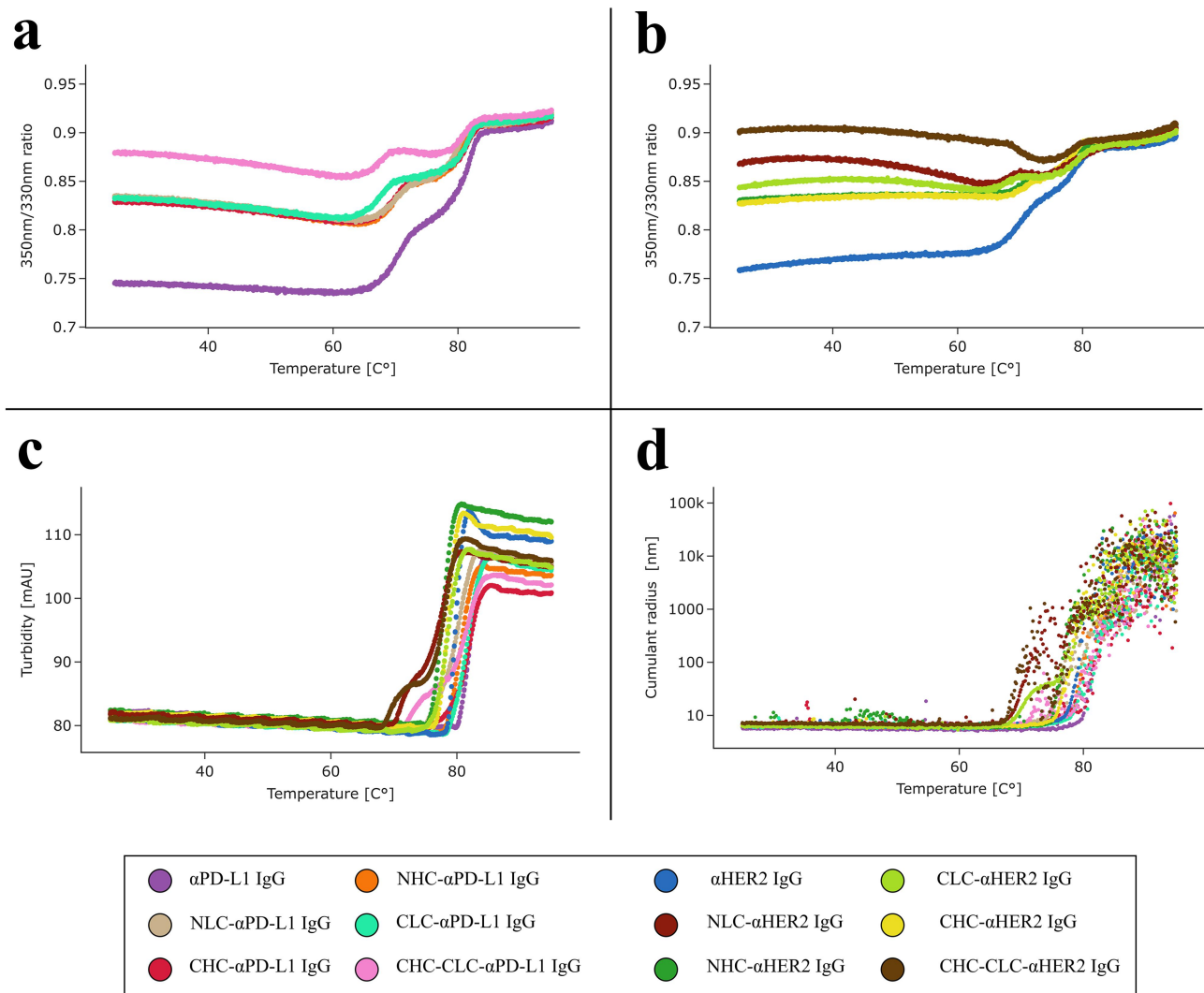


Figure 2. Biophysical stability of α PD-L1 α HER2 bsAbs. (a) DSF thermal scans showing 350nm/330nm fluorescence emission ratio for bsAbs based on the α PD-L1 IgG scaffold. (b) DSF thermal scans showing 350nm/330nm fluorescence emission ratio for bsAbs based on the α HER2 IgG scaffold. (c) Turbidity thermogram (measured with the backreflection optics) illustrating aggregation propensity in response to thermal unfolding. (d) DLS thermogram showing DLS cumulant radii in response to thermal unfolding.

reported as unfolding of CH2 (~70°C) and CH3 (~80°C), respectively.²⁹ The notable difference in the 350 nm/330 nm ratio prior to the unfolding transition for the bsAbs compared to the parent IgG1 most likely stems from the sdAbs containing surface-exposed tryptophan residues already in the fully folded state (Figure S4), thus increasing the 350 nm signal of the folded protein.

The sensitivity of DSF is illustrated by the ability to detect well-defined transition events at Tm1 (Figure 2a+) even though the absolute changes in fluorescence intensity at 350 nm are quite small (Figure S5). The small changes in absolute fluorescence intensity at 350 nm in response to CH2 unfolding suggest that no major changes in the local environment of tryptophan residues occurs during this structural transition. These findings indicate that the overall structural integrity of the antibodies is maintained after CH2 unfolding and highlight how DSF can be applied for understanding antibody stability against thermal unfolding.

The thermal stability of the CH3 domains, which is critical for proper HC pairing and overall structural integrity of the antibody molecule,^{30,31} appeared largely unaffected by the engineering for most of the bsAbs, as evidenced by similar Tm2 values between the bsAbs and their parent IgG1. The importance of the CH3 domains for antibody structural integrity and solubility is further illustrated in the turbidity profiles and DLS signals during the thermal ramp, where aggregation follows the unfolding of the CH3 domain, as seen in Figure 2. However, CH3 unfolding does not appear to be the sole determinant for aggregation. This is especially evident for the hexavalent bsAbs and NLC- α HER2, where small shoulders appear on the aggregation profile that precedes the main increase in turbidity despite Tm2 values that are comparable to the parent IgG1 molecules (Figure 2c+). The increased aggregation propensity of both hexavalent bsAbs shows that sdAb fusion affects the energetics of self-interaction, although the DLS cumulant radii do not show signs of self-interaction for any of the antibodies at lower temperatures. Further studies are needed to confirm the favorable developability profile at higher concentrations closer to those typically used when storing and administering therapeutic antibodies. Additionally, it is worth noting that the baselines of the turbidity- and DLS cumulant radii signals prior to aggregation (up to ca. 60°C) are very smooth, thus confirming the above-described high sample homogeneity even after only a single

purification step, and the essentially monomeric character of all the antibodies below the temperature range at which unfolding occurs.

Overall, we found the collected thermal stability profiles for all the bsAbs to be comparable to the parent IgG1 molecules, although sdAb fusion on the HC appeared to have a slightly lower impact on stability compared to LC fusion. The key measures from the thermal unfolding have been summarized in Table 2. Importantly, the simultaneous monitoring of aggregation during unfolding, as illustrated in Figure 2, favors in-depth understanding of the antibody behavior and developability profile. BsAb instabilities might have profound effects on the feasibility as a therapeutic agent and thorough analysis is thus required for proper candidate selection.

Evaluating bispecific *in vitro* binding functionality

For many bsAbs the functionality is based on the ability to simultaneously bind both targets to elicit effects that cannot be obtained with combinations of conventional monoclonal antibodies. Using our previously developed method based on flow-induced dispersion analysis (FIDA),¹⁶ we showed that exposure of the antibody panel to a fluorescently labeled (DY-490) detectable antigen \pm an unlabeled antigen yielded incremental increases in the apparent hydrodynamic radius (Rh). In this setup, FIDA only measures the apparent Rh of the fluorescently labeled antigen. Binding of bsAb to the fluorescent antigen will cause a change in apparent Rh due to complexation. The unlabeled antigen does not carry any fluorescence; hence it can only affect the signal indirectly through complexation with the bsAb, which is detected and measured through binding the other fluorescent antigen. This allows differentiation between whether the bsAb is complexed with one or both antigens. FIDA is an in-solution technique, and thus an ideal binding assay for structurally diverse bsAbs because the analysis does not rely on potentially obstructive surface immobilization and hence it is able to perform characterizations that are unbiased by bsAb format and spatial orientation of the binding domains. The results show that all investigated bsAbs can bind each target individually and both targets at the same time (Figure 3a+). The parent IgG1 and sdAb-Fc constructs both exhibited monospecific binding behavior, meaning that an Rh increase was only observed upon exposure to the first cognate antigen. The sizing experiment was performed using a so-called complex dissociation mixing approach,³² where pre-incubated complex is diluted

Table 2. Summary table containing stability parameters from the thermal ramping.

Antibody	Tm1 (°C)	Tm2 (°C)	Aggregation onset (°C)	Aggregation inflection point (°C)	Cumulant radius onset (°C)
α PD-L1 IgG	70.4	81.3	80.0	82.1	77.8
NHC- α PD-L1 IgG	69.7	80.4	77.6	80.5	72.7
CHC- α PD-L1 IgG	69.8	81.2	75.4	82.0	72.3
NLC- α PD-L1 IgG	70.0	79.6	74.2	80.4	71.4
CLC- α PD-L1 IgG	67.4	81.1	78.3	81.6	75.1
CHC-CLC- α PD-L1 IgG	67.2	80.8	70.9	81.7	69.5
α HER2 IgG	70.2	78.5	77.8	79.8	73.9
NHC- α HER2 IgG	70.4	77.5	75.3	77.7	73.4
CHC- α HER2 IgG	71.3	77.8	76.1	78.6	73.6
NLC- α HER2 IgG	67.8	78.3	69.6	77.8	66.7
CLC- α HER2 IgG	67.6	79.0	73.7	78.5	67.2
CHC-CLC- α HER2 IgG	70.0	78.3	68.2	78.2	66.3

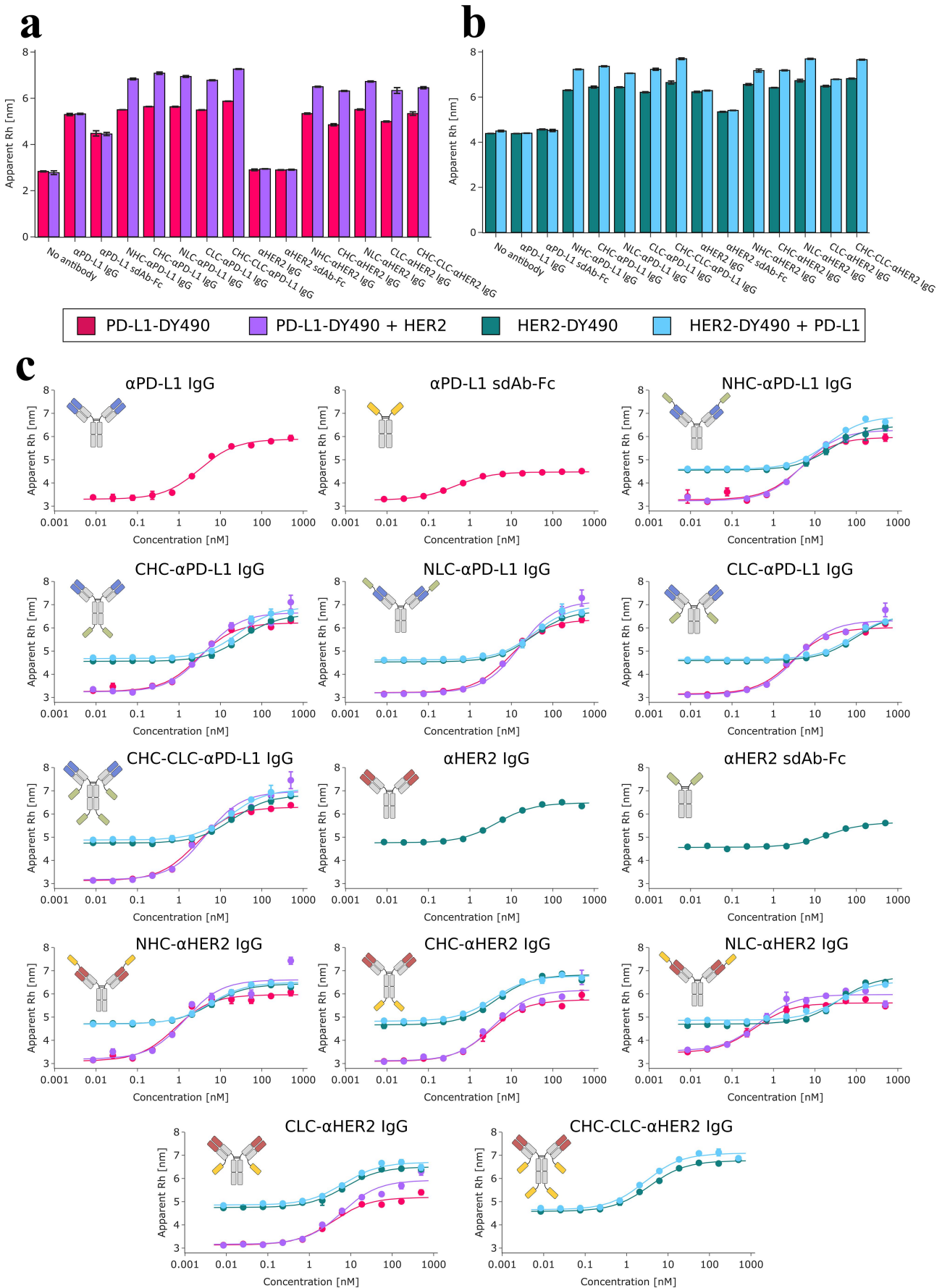


Figure 3. Antibody binding to PD-L1 and HER2 using FIDA. (a) Assessment of bispecific binding functionality through changes in apparent Rh in response to addition of fluorescent PD-L1-DY490 \pm unlabeled HER2 antigens in solution (b) Assessment of bispecific binding functionality through changes in apparent Rh in response to addition of fluorescent HER2-DY490 \pm unlabeled PD-L1 antigens in solution. (c) Antibody titration curves investigating binding in mono- and bispecific binding environments. The binding curves were generated by titrating antibody against the fluorescently labeled primary antigen \pm an unlabeled secondary antigen. Since the secondary antigen does not carry any fluorescence, it can only affect the signal indirectly through complexation with the bsAb, which is in itself binding the primary antigen. This is to test if the titration curves change in response to addition of the unlabeled secondary antigen. The coloring scheme is the same as in (a) and (b).

in assay buffer inside the capillary to induce dissociation. The result showed that the bispecific ternary complex is formed, and it appears to be stable throughout the analysis window (approx. 2 min). Overall, the observed Rh values suggest that sdAbs can be fused in all the investigated positions to form functionally bispecific antibodies capable of binding both antigens simultaneously. Lastly, the observed apparent Rh values confirm the larger expected MW of HER2 (70.2 kDa) compared to PD-L1 (26.0 kDa), thus further supporting the above mentioned correlation between molecular size and theoretical MW. The expected correlation between MW and apparent Rh should in principle allow probing of the average number of occupied binding sites. Figure 3a+b shows that the hexavalent bsAbs exhibit similar increases in Rh as the tetravalent bsAbs even though they have been engineered to contain more available binding sites. This could indicate that the hexavalent bsAbs are not able to utilize all their available binding sites at the same time. However, considering that both the tetravalent CHC- and CLC constructs exhibit bispecific binding functionally, it seems more likely that the excess of binding sites in the reaction are competing for the antigen, and thus preventing formation of higher order complexes where all binding sites are occupied at the same time.

We further used FIDA for quantitative assessment of binding affinity constants (K_D) of the antibody panel against the individual antigens in both a monospecific and bispecific binding environment (Figure 3c and Table 3). We found that the observed affinity constants for the individual antigen-binding domains (Fv and sdAb) when included in the bsAbs are generally comparable to those reported when the domains were analyzed as conventional monospecific antibody

constructs.^{20,21,33,34} It should be noted that these previously reported affinities were not obtained using FIDA and the results might therefore not be fully comparable to this work, although the affinity values are still highly similar. From the binding affinity constants, fusion of sdAb N-terminally onto the LC introduces a risk of impairing binding functionality of the scaffold Fv, most likely due to steric hindrance. This is especially evident from the construct where α PD-L1 sdAb is fused N-terminally to the LC of α HER2 IgG1 (NLC- α HER2 IgG), which has an affinity almost 8-fold lower than the parent α HER2 IgG1. Interestingly, the same reduction in HER2 binding was not observed when the α PD-L1 sdAb was fused to the N-terminus of the HC of the α HER2 IgG1 (NHC- α HER2 IgG), even though the two N-termini are expected to be spatially close. Additionally, sdAb fusion C-terminally to the LC appears to be associated with a reduction in binding affinity of the fused sdAb. As an example, fusion of α HER2 sdAb C-terminally to the LC of α PD-L1 IgG1 (CLC- α PD-L1 IgG) shows a reduced affinity toward HER2 compared to the monospecific α HER2 sdAb-Fc construct. Again, the decrease in affinity appears less pronounced for C-terminal fusion on HC compared to C-terminal fusion on LC. As mentioned above, all sdAbs were fused using a flexible 10-aa GS linker. The length of the linker is likely to affect the spatial sdAb arrangement, hence different linkers might affect the binding affinities.

The apparent reductions in binding affinities are consistent across “specificity orientations”, indicating that the observed effects are caused by the molecular geometry rather than effects related to the unique antibody-antigen interaction. Furthermore, the impaired binding can be seen for both

Table 3. Affinity binding constants and the related goodness-of-fit from antibody titration curves using FIDA. The titration curves were generated by titrating antibodies against a fluorescently labeled antigen \pm the unlabeled antigen. The goodness-of-fit is evaluated using R^2 and root mean squared error (RMSE). Affinity values in brackets marked with an asterisk indicate affinity values previously reported elsewhere.^{20,21,33,34}

Antibody	PD-L1-DY490		PD-L1-DY490 + HER2		HER2-DY490		HER2-DY490 +PD-L1	
	K_D (nM)	Goodness-of-fit	K_D (nM)	Goodness-of-fit	K_D (nM)	Goodness-of-fit	K_D (nM)	Goodness-of-fit
α PD-L1 IgG	1.8 (1.8*)	$R^2=0.994$ RMSE=0.12	N/A	N/A	N/A	N/A	N/A	N/A
α PD-L1 sdAb-Fc	0.3 (3.0*)	$R^2=0.999$ RMSE=0.05	N/A	N/A	N/A	N/A	N/A	N/A
NHC- α PD-L1 IgG	2.4	$R^2=0.985$ RMSE=0.16	2.6	$R^2=0.995$ RMSE=0.1	17.9	$R^2=0.993$ RMSE=0.14	14.3	$R^2=0.993$ RMSE=0.08
CHC- α PD-L1 IgG	1.6	$R^2=0.993$ RMSE=0.12	2.0	$R^2=0.982$ RMSE=0.23	22.3	$R^2=0.997$ RMSE=0.05	19.0	$R^2=0.986$ RMSE=0.13
NLC- α PD-L1 IgG	4.6	$R^2=0.994$ RMSE=0.11	7.1	$R^2=0.993$ RMSE=0.18	21.6	$R^2=0.987$ RMSE=0.15	23.6	$R^2=0.990$ RMSE=0.14
CLC- α PD-L1 IgG	1.5	$R^2=0.992$ RMSE=0.11	1.8	$R^2=0.980$ RMSE=0.21	66.1	$R^2=0.995$ RMSE=0.06	57.9	$R^2=0.994$ RMSE=0.06
CHC-CLC- α PD-L1 IgG	1.3	$R^2=0.995$ RMSE=0.11	2.0	$R^2=0.981$ RMSE=0.26	13.7	$R^2=0.998$ RMSE=0.07	12.3	$R^2=0.992$ RMSE=0.13
α HER2 IgG	N/A	N/A	N/A	N/A	3.3 (2.8*)	$R^2=0.995$ RMSE=0.06	N/A	N/A
α HER2 sdAb-Fc	N/A	N/A	N/A	N/A	16.2 (11.6*)	$R^2=0.991$ RMSE=0.07	N/A	N/A
NHC- α HER2 IgG	0.4	$R^2=0.985$ RMSE=0.17	0.7	$R^2=0.949$ RMSE=0.35	4.5	$R^2=0.994$ RMSE=0.08	4.2	$R^2=0.998$ RMSE=0.07
CHC- α HER2 IgG	1.6	$R^2=0.991$ RMSE=0.15	1.9	$R^2=0.971$ RMSE=0.25	2.9	$R^2=0.990$ RMSE=0.11	2.6	$R^2=0.997$ RMSE=0.07
NLC- α HER2 IgG	0.2	$R^2=0.993$ RMSE=0.12	0.3	$R^2=0.974$ RMSE=0.21	26.0	$R^2=0.985$ RMSE=0.10	26.4	$R^2=0.981$ RMSE=0.09
CLC- α HER2 IgG	2.3	$R^2=0.985$ RMSE=0.12	3.3	$R^2=0.978$ RMSE=0.19	5.2	$R^2=0.994$ RMSE=0.09	4.8	$R^2=0.987$ RMSE=0.11
CHC-CLC- α HER2 IgG	N/A	N/A	N/A	N/A	2.4	$R^2=0.998$ RMSE=0.06	1.8	$R^2=0.993$ RMSE=0.10

Table 4. Steady-state K_D measurements of antibody binding to Fc γ IIIa using BLI analysis.

Antibody	K_D (μ M)	Goodness-of-fit
α PD-L1 IgG	0.52	$R^2=0.99$
NHC- α PD-L1 IgG	0.56	$R^2=0.99$
CHC- α PD-L1 IgG	0.57	$R^2=0.99$
NLC- α PD-L1 IgG	0.44	$R^2=0.99$
CLC- α PD-L1 IgG	0.41	$R^2=0.99$
CHC-CLC- α PD-L1 IgG	0.67	$R^2=0.99$
α HER2 IgG	0.54	$R^2=0.99$
NHC- α HER2 IgG	1.10	$R^2=0.99$
CHC- α HER2 IgG	0.64	$R^2=0.99$
NLC- α HER2 IgG	0.40	$R^2=0.99$
CLC- α HER2 IgG	0.43	$R^2=0.99$
CHC-CLC- α HER2 IgG	0.44	$R^2=0.99$

mono- and bispecific binding setups, which further supports that it is the molecular architecture that imposes the binding restraints. The results demonstrate FIDA as an ideal option for quantifying binding functionality of bsAbs with diverse molecular architectures. FIDA is an immobilization-free technique, and thus enables characterizations that are not biased by geometrical restraints which may occur through immobilization of the bsAb. This is crucial considering that bsAb functionality is highly dependent on an optimal molecular format. On the other side, FIDA, as an in-solution assay, might not account for geometrical restraints imposed by cell surfaces on cell surface receptors. For bsAbs targeting surface-associated moieties, such as T-cell redirecting bsAbs,³⁵ additional assays would be needed to ensure that the format supports optimal binding geometry for simultaneous binding of cell surface-associated antigens on two different cells.

Effect of engineering on effector functions

For many therapeutic antibodies, Fc-mediated effector functions contribute to, and are necessary for, the desired therapeutic response. For example, binding of Fc to Fc γ RIIIa (CD16a) on NK cells mediates antibody-dependent cellular cytotoxicity (ADCC) of target cells whereby the killing activity correlates positively to the affinity of Fc with Fc γ RIIIa.³⁶ Using BLI we investigated equilibrium dissociation constants of our antibody panel against Fc γ RIIIa (allotype 176F) to assess if sdAb fusion affected Fc γ RIIIa receptor binding of the bsAbs compared to the parent IgG1. BLI was chosen over FIDA because preliminary experiments indicated that the fluorescence labeling procedure affected the antibody:Fc γ IIIa interaction, likely based on lysine residues present in the binding interface of Fc and Fc γ RIIIa (data not shown).

Steady-state K_D measurements for binding of the antibody panel to Fc γ RIIIa are shown in Table 4. We chose the steady-state K_D measurements over the full kinetic analysis because Fc γ RIIIa is a low-affinity receptor with a high on-rate, for which accurate estimation of kinetic parameters can be difficult (full sensorgrams are shown in Figure S6). From the observed K_D measurements, the engineered molecular formats generally do not appear to have any detrimental effects on Fc γ RIIIa receptor binding. One exception is the NHC- α HER2 IgG, where the affinity appears to notably decrease compared to the parent IgG1. Since the same decrease in affinity is not observed for NHC- α PD-

L1 IgG, the change in binding affinity does not appear to be caused by the general molecular geometry, but depends to the particular sdAb. The observed affinities were generally in agreement with previously reported values for IgG1 Fc binding to Fc γ IIIa (176F) using BLI and immobilization via the Fab domain.³⁷

Discussion

BsAbs represent a unique class of antibody-based therapeutics with modes of action (MoA) beyond those of conventional monoclonal antibodies. While bsAbs are highly attractive as therapeutic agents, their design, production, and analysis are often complicated by complex molecular formats. Most clinically developed antibodies follow an asymmetric architecture with up to four different antibody chains, thereby deviating from the conventional HC₂LC₂ format,⁸ and typically the chains have been engineered for steering polypeptide chain pairing⁴ or selective purification to obtain the desired heterodimeric bsAb product.⁹ In spite of engineering efforts, optimal conditions for expression of high-quality asymmetric bsAbs can be difficult to obtain³⁸ and might differ between different bsAbs,³⁹ thus increasing the risk of mispaired product-related impurities. Furthermore, an increasing number of bsAbs aim to include bivalent binding for each specificity, similar to that achieved by standard antibodies for one specificity. In this work, we show that genetic fusion of sdAbs onto IgG1 scaffolds is a robust strategy for the formation of high-quality IgG-like bsAbs using highly effective routine workflows for production and purification of monoclonal antibodies. Previously, scFvs have been used for fusion to IgG scaffolds, but the resulting fusion constructs are often prone to self-assembly and formation of high MW aggregates,¹³ even after stability engineering of the scFv components.¹⁴ In contrast, sdAbs are robust and monomeric in nature and are thus unlikely to self-assemble or aggregate while folded, which is in agreement with our reported results. We investigated a panel of IgG-like bsAbs, IgG1-sdAb fusions with diverse molecular formats, and found that these could be effectively produced using routine methods and an effective one-step protein A-based purification. The bsAb molecular architecture was found to have a profound effect on the expression yields, with sdAb fusions to the HC being advantageous compared to sdAb-fusions to the LC. Interestingly, sdAb fusion to the HC in N-terminal or C-terminal configuration lead in all cases to

an expression higher than the parental IgG1, while the fusion of sdAb to the LC in most cases showed lower expression than the parental IgG1. The symmetric nature of the bsAbs mean that these could all be produced using standard workflows of monoclonal antibodies with very little optimization of, for example, plasmid transfection ratios that are normally needed for asymmetric bsAbs. Symmetric molecular geometry, however, also means that the antigen-binding domains will always appear in pairs. Asymmetric solutions are thus critical, because, while bivalent binding can be advantageous for some bsAb, in many cases monovalency of at least one binding specificity, such as anti-CD3, is desired.

In assessing the homogeneity and stability of our antibody panel, we found that the various bsAbs constructs generally showed thermodynamic stabilities and aggregation propensities that were similar to the parent IgG1 molecules. We expect that the favorable stability profiles are connected to the CH3 domain, which is important for antibody structural integrity, and remained un-engineered for the investigated bsAb panel. In contrast, most platforms for HC heterodimerization of asymmetric bsAbs are based on engineering of the CH3 domains, which is known to negatively affect the thermal stability.^{40–43} Although the structural integrity of antibodies is believed to be tightly linked to proper pairing of intact CH3 domains, we found that some of the bsAbs started aggregating prior to CH3 unfolding. This indicates that the colloidal stability of structurally complex bsAbs is not only dependent on the structural integrity of the individual domains, but that the sdAb fusion itself will also affect the aggregation propensity of the bsAb. Accordingly, two of the most aggregation-prone antibodies in our study were the hexavalent bsAbs where four individual sdAbs had been fused onto the IgG scaffold.

The MoA of many bsAbs relies on simultaneous engagement of both targets. Using FIDA, we were able to show that

the bsAbs are not only capable of binding each antigen individually, but that they can also be bound at the same time, thus making the bsAbs functionally bispecific. FIDA was chosen over traditional surface-based techniques, since it allows selective and differential characterization of bsAb binding to a single antigen as well as simultaneous binding of both antigens.¹⁶ FIDA does not rely on immobilization chemistries, thus rendering the analysis unaffected by potential steric effects introduced through immobilization of the various antibody architectures.

Affinity measurements of the antibody panel against both antigens indicate that molecular geometry affects the bsAb binding strength, most likely because sdAb fusion risks introducing steric restraints on the individual binding domains. When fusing sdAbs N-terminally onto the IgG1 scaffold, a steric restraint is placed on the Fv domain, which is to some extent blocked by the fused sdAb domain. Interestingly, fusion of the sdAb to the N-terminus of the LC seemed to impose more steric restraint than sdAb fusion to the N-terminus of the HC, even though the two N-termini are expected to be spatially close. Examination of a crystal structure of trastuzumab in complex with HER2, however, revealed that the N-terminus of the LC is located closer to the paratope than the corresponding HC N-terminus (Figure 4a). This could explain how sdAb fusion to the N-terminus of HC and LC, respectively, may introduce two different levels of steric hindrance. The antibody fold is a highly conserved structural domain outside the hypervariable loops, and hence it is likely that the HC N-terminus will generally be further away from the paratope than the N-terminus of the LC. In contrast, when fusing sdAbs C-terminally on the IgG1 scaffold the impaired binding was observed for the fused sdAb. We expect this to be because the N-terminus of sdAbs (and other VH domains) are oriented in roughly the same direction as the complementary-

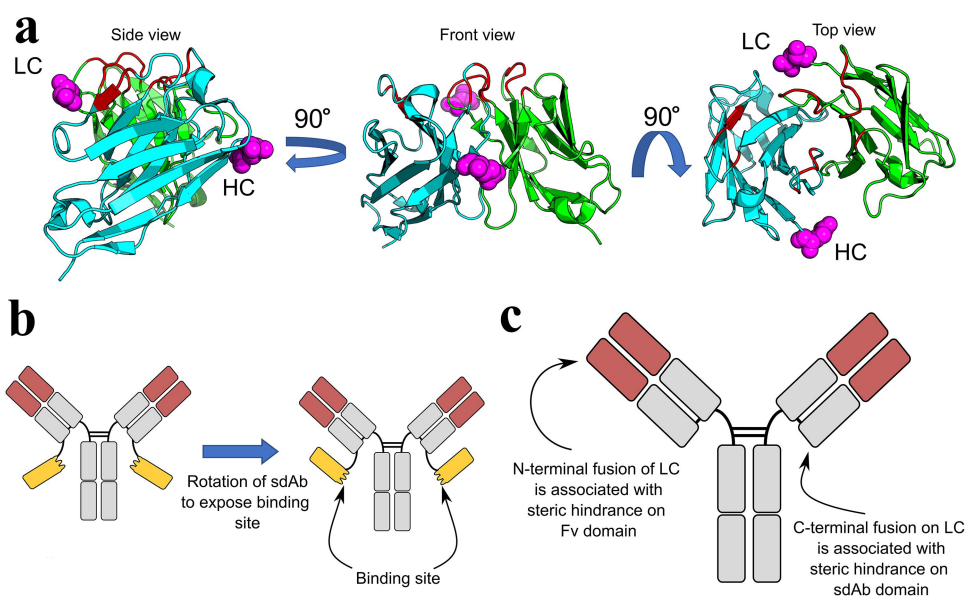


Figure 4. Interpreting the effect of bsAb molecular geometry on binding affinities. (a) Ribbon representation of Trastuzumab Fv (PDB: 1N8Z) showing positions of N-termini of HC (cyan) and LC (green) relative to the antigen-binding paratope. The N-termini are indicated with magenta ball representation. The paratope (red) have been approximated as those residues that are within 6 Å of the HER2 antigen in the complex (antigen not shown). (b) Schematic illustration of the expected sdAb rotation required for exposing the paratope when the sdAb is fused C-terminally to the LC of the IgG1 scaffold. (c) Schematic summary of potential steric restraints introduced when fusing sdAbs on LC of IgG1 scaffold.

determining regions that mediate antigen binding. Fusing the sdAb C-terminally on an IgG chain therefore means that the sdAb binding interface is oriented inwards toward the scaffold, and hence the sdAbs must rotate to properly expose its paratope for antigen binding (Figure 4b).

The presence of an Fc region could sterically limit the sdAb rotation and access of the antigen, and thus explain why a reduction in sdAb binding affinity is not as pronounced for C-terminal fusions to HC as for C-terminal fusions to LC. It may be possible that linkers other than the 10-aa (GGGS)₂ linker used in this study could alleviate some of the steric restraints for both N-terminal and C-terminal fusion by allowing more space and flexibility for re-orienting the sdAb. Additional studies under physiological conditions may further confirm the stability of GS linkers and the molecule as a whole under these conditions. The main effects on antigen binding affinity from fusion of sdAbs onto IgG1 scaffolds are summarized in Figure 4c. In addition to antigen binding, we further investigated if the Fc effector functions were intact for the engineered bsAbs. Using FcγRIIIa as a model receptor, we did not find that any of the tested sdAb fusion formats has an effect on Fc binding to the FcγRIIIa receptor, which is a prerequisite for ADCC-mediated cell killing. Further studies will be needed to address comparative FcRn-mediated recirculation and half-life of the antibody formats.

Taken together, our study provides a flexible framework for generating robust and stable bsAbs by combining sdAbs and IgG1 to form symmetric bsAbs with diverse molecular architectures and valencies that can be selected to suit the biological function. The majority of the tested bsAbs in our antibody panel were tetravalent (bivalent for each antigen), as we believed these antibodies would most closely resemble the bivalent binding of conventional IgG antibodies. This is, to the best of our knowledge, the most comprehensive comparison of sdAb-IgG bsAb architectures yet. Fusion of sdAbs represents a strong alternative to the traditional scFv-IgG bsAbs, mainly because sdAbs are naturally small monomeric binding domains and thus: 1) are highly modular, 2) are unlikely to self-associate and mispair, and 3) can be easily reformatted to fragments from full-length IgG with low risk of losing activity. In agreement with previous reports, we find that the molecular geometry of the bsAb has a clear impact on the production and functionality of the bsAbs, with our findings suggesting that sdAb fusion on HC (both N-terminally and C-terminally) is generally advantageous compared to fusion on LC. The findings were consistent for both groups of bsAb geometries with reversely mirrored specificities (αHER2 sdAb fused to αPD-L1 IgG and αPD-L1 sdAb fused to αHER2 IgG, respectively), thus indicating that the observations are rooted in the structural format. It should be noted that, although our antibody panel was comprehensively tested for *in vitro* binding functionality and biophysical stability, the cellular activity, where the molecular geometry is also expected to play a significant role,^{6,7} was not investigated in this study. Lastly, the work presents a toolbox of analytical techniques that can be used for capturing the increased complexity of bsAbs compared to conventional monoclonal antibodies for improved candidate selection and drug discovery campaigns. We expect that our findings will help advance the design and development of novel bsAbs.

Materials and methods

Production of bispecific antibodies

The design and production of symmetric bsAbs were done as previously reported using a two-plasmid system.¹⁶ In brief, genes encoding antibody variable domains or sdAb domains were obtained from Twist BioScience and cloned into pcDNA3.1-based expression vectors containing either IgG1 constant domains for HC vectors or C_κ for LC vectors. The sdAb genes were linked to the IgG scaffold through a flexible (GGGS)₂ linker. The antibodies were produced by co-transfecting HC and LC plasmids (3:2 ratio) in HEK293F cells and culturing for 7 days in FreeStyle™ 293 Expression Medium (ThermoFisher) at 37°C and 5% CO₂ in shake flasks. All antibodies were expressed in triplicates except for the two hexavalent antibodies with fusion on both HC and LC. The supernatants were clarified by centrifugation (1500×g for 10 min) and filtering (0.45 μm) and the triplicate cultures were pooled before loading on HiTrap MabSelect SuRe column (Cytiva) connected to an ÄKTA Pure system (Cytiva). The yields after purification were calculated using an in-house developed Python script and theoretical extinction coefficient predicted by ProtParam (ExPASy) based on the amino acid sequence of fully assembled monomeric antibodies.⁴⁴ All the antibodies were concentrated and buffer exchanged to phosphate-buffered saline (PBS) using Amicon Ultra-15 centrifugal filter devices (30-kDa cutoff, EMD) and the protein concentrations were measured using NanoDrop One UV-Vis spectrophotometer (ThermoFisher).

Octet BLI quantitation

The antibody concentrations in crude supernatant were determined using an Octet RED96e platform (FortéBio). ProA biosensors (Sartorius) were pre-wetted in fresh culture medium before a 1-step direct quantitation using dip and read for 120 s. The data was fitted using a pre-calculated rituximab standard curve (6.25–300 μg/mL) and the default 4PL equation using Octet data analysis software (Sartorius).

SDS-PAGE

The quality of the purified antibodies was analyzed by SDS-PAGE (4–20% Mini-PROTEAN® TGX™ Precast Protein Gels, Bio-Rad) in the presence and absence of 25 mM 1,4-dithiothreitol (DTT) and visualized through Coomassie Brilliant Blue staining. Precision Plus Protein Dual Color Standards (Bio-Rad, #1610374) was included as reference.

Capillary electrophoresis

Capillary electrophoresis was performed using the High Sensitivity Protein 250 kit (Agilent) with an Agilent 2100 BioAnalyzer according to manufacturer protocol without any reducing agent. The 2100 Expert software (Agilent, v. B.02.11. S1824) was used for size calling and relative quantification of the peaks. Only peaks representing ≥2% of total protein sample content were included in the analysis.

Size exclusion chromatography

For analytical SEC we used a Superdex Increase 200 5/150 GL column (Cytiva) connected to ÄKTA Pure system (Cytiva). The running buffer was PBS (2.67 mM KCl, 1.47 mM KH₂PO₄, 137.9 mM NaCl, 8.1 mM Na₂PO₄). The amount of aggregation was calculated using the above-mentioned Python script. Separation of the aggregation peak from monomeric peak was done based on local minima determined through the first derivative of the chromatogram.

Sizing and thermal stability

Particle sizing and thermal stability were analyzed by running DLS and DSF with a Prometheus Panta equipped with backreflection optics (NanoTemper Technologies). The DLS sizing analysis utilized light scattering at 405 nm with a photomultiplier tube in a backscatter orientation and with a solvent refractive index of 1.335. For assessment of thermal stability, the antibodies were analyzed by DSF (including backreflection) and DLS while subjected to thermal ramping at 1.0°C/min from 25°C to 95°C. We used high sensitivity capillaries (NanoTemper Technologies) and antibodies at 0.35–0.4 mg/mL for all sizing and thermostability experiments. Analysis of experimental data was performed using the Prometheus Panta Control Software (NanoTemper Technologies).

FIDA analysis

The FIDA experiments were performed as previously described.¹⁶ In brief, we used a FIDA One instrument employing light-emitting diode-induced fluorescence detection using an excitation wavelength of 480 nm and an emission wavelength of >515 nm (Fida Biosystems). The PD-L1 (ACRO Biosystem, #PD1-H5229) and HER2 (ACRO Biosystems, #HE2-H5225) antigens were fluorescently labeled with DY-490 (EMP Biotech, #MKD0125) and the assay buffer was PBS+0.1% bovine serum albumin (BSA). Affinity measurements were performed in capmix mode by initial loading of the capillary with antibody solution at varying concentrations (3500 mbar, 20s), then injecting 20 nM fluorescent indicator ± equimolar unlabeled antigen (50 mbar, 10s), and finally a second loading step with antibody (400 mbar, 180–200s). Sizing of antibody complexes was performed in a complex dissociation mode by loading buffer (3500 mbar, 20s), then injecting a pre-mixed (>15 min) solution with 32 nM fluorescent antigen and 40 nM antibody ± 80 nM unlabeled antigen (50 mbar, 10s), followed by a second buffer loading (400 mbar, 180–200s). A flush with assay buffer (3500 mbar, 120s) was performed between each measurement. Rh values were obtained by Taylorgrams to FIDA Software v2.3 (Fida Biosystems) with a Taylorgram fraction of 75%. The titration curves were fitted to a simple 1:1 binding using our in-house Python script.

Octet BLI Fcγ receptor binding

Binding of bsAb and IgG to monomeric FcγIIIa (CD16A)-176F (ACRO Biosystem, #CDA-H5220) was measured using an Octet RED96e (FortéBio). Antibodies were diluted to 5 µg/mL in assay buffer (PBS pH 7.4, 0.02% Tween20, 0.1% BSA) and immobilized on FAB2G biosensors (Sartorius) for 120 s followed by 180 s washing in assay buffer. The antibodies were then associated to FcγIIIa (0–500 nM) for 60 s followed by 60 s dissociation in assay buffer. The sensorgrams were fitted globally using our in-house developed Python script assuming a 1:1 binding model. The entire association step and the 5 first seconds of the dissociation step were used in the fitting.

Data analysis

The data was compiled into Microsoft Excel and analyzed using an in-house developed Python script (available through https://github.com/andreasvisbech/Plotly_data_analysis/releases/tag/3.3.0) unless otherwise stated. We prioritized using the Python script for analysis when possible, to promote transparency and reproducibility in the data analysis. The Excel files with raw data and the parameter log files are available in the supplemental online material.

Abbreviations

ADCC	antibody dependent cellular cytotoxicity
BLI	biolayer interferometry
bsAb	bispecific antibody
CE	capillary electrophoresis
DLS	dynamic light scattering
DSF	differential scanning fluorimetry
FIDA	flow-induced dispersion analysis
Fv	variable region
HC	heavy chain
HER2	human epidermal growth factor receptor 2
IgG	immunoglobulin G
K _D	binding affinity constant
LC	light chain
MoA	mode-of-action
MW	molecular weight
PD-L1	Programmed Cell Death Ligand 1
Rh	hydrodynamic radius
RMSE	root mean squared error;
scFv	single-chain variable region
sdAb	single-domain antibody
SEC	size exclusion chromatography

Acknowledgments

We thank employees at FidaBio for discussions on FIDA analysis.

Disclosure statement

No potential conflict of interest was reported by the authors.

Funding

This work was supported by The Novo Nordisk Foundation Grants NNF19SA0056783, NNF19SA0057794, and NNF20SA0066621.

ORCID

Andreas V. Madsen  <http://orcid.org/0000-0002-8449-9691>

Peter Kristensen  <http://orcid.org/0000-0001-7205-6853>

Alexander K. Buell  <http://orcid.org/0000-0003-1161-3622>

Steffen Goletz  <http://orcid.org/0000-0003-1463-5448>

References

- Sampei Z, Igawa T, Soeda T, Okuyama-Nishida Y, Moriyama C, Wakabayashi T, Tanaka E, Muto A, Kojima T, Kitazawa T, et al. Identification and multidimensional optimization of an asymmetric bispecific IgG antibody mimicking the function of factor VIII cofactor activity. *Plos One*. 2013;8:e57479. doi:10.1371/journal.pone.0057479.
- McDonagh CF, Huhlov A, Harms BD, Adams S, Paragas V, Oyama S, Zhang B, Luus L, Overland R, Nguyen S, et al. Antitumor activity of a novel bispecific antibody that targets the ErbB2/ErbB3 oncogenic unit and inhibits heregulin-induced activation of ErbB3. *Mol Cancer Ther*. 2012;11:582–93. doi:10.1158/1535-7163.MCT-11-0820.
- Wec AZ, Nyakatura EK, Herbert AS, Howell KA, Holtsberg FW, Bakken RR, Mittler E, Christin JR, Shulenin S, Jangra RK, et al. A “Trojan horse” bispecific-antibody strategy for broad protection against ebolaviruses. *Science*. 2016;354:350–54. doi:10.1126/science.aag3267.
- Brinkmann U, Kontermann RE. The making of bispecific antibodies. *Mabs*. 2017;9:182–212. doi:10.1080/19420862.2016.1268307.
- Dickopf S, Georges GJ, Brinkmann U. Format and geometries matter: structure-based design defines the functionality of bispecific antibodies. *Comput Struct Biotechnol J*. 2020;18:1221–27. doi:10.1016/j.csbj.2020.05.006.
- Kast F, Schwill M, Stüber JC, Pfundstein S, Nagy-Davidescu G, Rodríguez JMM, Seehusen F, Richter CP, Honegger A, Hartmann KP, et al. Engineering an anti-HER2 biparatopic antibody with a multimodal mechanism of action. *Nat Commun*. 2021;12:3790. doi:10.1038/s41467-021-23948-6.
- Croasdale R, Wartha K, Schanzer JM, Kuenkele KP, Ries C, Mayer K, Gassner C, Wagner M, Dimoudis N, Herter S, et al. Development of tetravalent IgG1 dual targeting IGF-1R–egfr antibodies with potent tumor inhibition. *Arch Biochem Biophys*. 2012;526:206–18. doi:10.1016/j.abb.2012.03.016.
- Labrijn AF, Janmaat ML, Reichert JM, Parren PWI. Bispecific antibodies: a mechanistic review of the pipeline. *Nat Rev Drug Discov*. 2019;18:585–608. doi:10.1038/s41573-019-0028-1.
- Li Y. A brief introduction of IgG-like bispecific antibody purification: methods for removing product-related impurities. *Protein Expr Purif*. 2019;155:112–19. doi:10.1016/j.pep.2018.11.011.
- Chen SW, Zhang W. Current trends and challenges in the downstream purification of bispecific antibodies. *Antib Ther*. 2021;4:73–88. doi:10.1093/abt/tbab007.
- Dengl S, Mayer K, Bormann F, Duerr H, Hoffmann E, Nussbaum B, Tischler M, Wagner M, Kuglstatler A, Leibrock L, et al. Format chain exchange (FORCE) for high-throughput generation of bispecific antibodies in combinatorial binder-format matrices. *Nat Commun*. 2020;11:4974. doi:10.1038/s41467-020-18477-7.
- Wörn A, Plückthun A. Stability engineering of antibody single-chain Fv fragments. *J Mol Biol*. 2001;305:989–1010. doi:10.1006/jmbi.2000.4265.
- Michaelson JS, Demarest SJ, Miller B, Amatucci A, Snyder WB, Wu X, Huang F, Phan S, Gao S, Doern A, et al. Anti-tumor activity of stability-engineered IgG-like bispecific antibodies targeting TRAIL-R2 and LTβR. *Mabs*. 2009;1:128–41. doi:10.4161/mabs.1.2.7631.
- Cao M, Wang C, Chung WK, Motabar D, Wang J, Christian E, Lin S, Hunter A, Wang X, Liu D. Characterization and analysis of scFv-IgG bispecific antibody size variants. *Mabs*. 2018;10:1236–47. doi:10.1080/19420862.2018.1505398.
- Muyldermans S. Nanobodies: natural single-domain antibodies. *Annu Rev Biochem*. 2013;82:775–97. doi:10.1146/annurev-biochem-063011-092449.
- Madsen AV, Mejias-Gomez O, Pedersen LE, Skovgaard K, Kristensen P, Goletz S. Immobilization-Free binding and affinity characterization of higher order bispecific antibody complexes using size-based microfluidics. *Anal Chem*. 2022;94:13652–58. doi:10.1021/acs.analchem.2c02705.
- Irving B, Chiu H, Maecker H, Mariathasan S, Lehar S, Wu Y, Cheung J, inventors; Genentech, assignee. Anti-PD-L1 Antibodies, Compositions and Articles of Manufacture. United States patent US8217149B2. 2012 July 10.
- Powles T, Eder JP, Fine GD, Braiteh FS, Loriot Y, Cruz C, Bellmunt J, Burris HA, Petrylak DP, Teng SL, et al. MPDL3280A (anti-PD-L1) treatment leads to clinical activity in metastatic bladder cancer. *Nature*. 2014;515:558–62. doi:10.1038/nature13904.
- Cho HS, Mason K, Ramyar KX, Stanley AM, Gabelli SB, Denney DW, Leahy DJ. Structure of the extracellular region of HER2 alone and in complex with the Herceptin Fab. *Nature*. 2003;421:756–60. doi:10.1038/nature01392.
- Zhang F, Qi X, Wang X, Wei D, Wu J, Feng L, Cai H, Wang Y, Zeng N, Xu T, et al. Structural basis of the therapeutic anti-PD-L1 antibody atezolizumab. *Oncotarget*. 2017;8:90215–24. doi:10.18632/oncotarget.21652.
- Vaneycken I, Devoogdt N, Van Gassen N, Vincke C, Xavier C, Wernery U, Muyldermans S, Lahoutte T, Caveliers V. Preclinical screening of anti-HER2 nanobodies for molecular imaging of breast cancer. *Faseb J*. 2011;25:2433–46. doi:10.1096/fj.10-180331.
- Dimasi N, Fleming R, Wu H, Gao C. Molecular engineering strategies and methods for the expression and purification of IgG1-based bispecific bivalent antibodies. *Methods*. 2019;154:77–86. doi:10.1016/j.ymeth.2018.08.004.
- Yanakieva D, Pekar L, Evers A, Fleischer M, Keller S, Mueller-Pompalla D, Toleikis L, Kolmar H, Zielonka S, Krah S. Beyond bispecificity: controlled Fab arm exchange for the generation of antibodies with multiple specificities. *Mabs*. 2022;14:2018960. doi:10.1080/19420862.2021.2018960.
- Wu X, Sereno AJ, Huang F, Lewis SM, Lieu RL, Weldon C, Torres C, Fine C, Batt MA, Fitchett JR, et al. Fab-based bispecific antibody formats with robust biophysical properties and biological activity. *Mabs*. 2015;7:470–82. doi:10.1080/19420862.2015.1022694.
- Lavoisier A, Schlaeppli JM. Early developability screen of therapeutic antibody candidates using Taylor dispersion analysis and UV area imaging detection. *Mabs*. 2015;7:77–83. doi:10.4161/19420862.2014.985544.
- Smilgies DM, Folta-Stogniew E. Molecular weight-gyration radius relation of globular proteins: a comparison of light scattering, small-angle X-ray scattering and structure-based data. *J Appl Crystallogr*. 2015;48:1604–06. doi:10.1107/S1600576715015551.
- Jain T, Sun T, Durand S, Hall A, Houston NR, Nett JH, Sharkey B, Bobrowicz B, Caffry I, Yu Y, et al. Biophysical properties of the clinical-stage antibody landscape. *Proc Natl Acad Sci U S A*. 2017;114:944–49. doi:10.1073/pnas.1616408114.
- Kim SH, Yoo HJ, Park EJ, Na DH. Nano differential scanning fluorimetry-based thermal stability screening and optimal buffer selection for immunoglobulin G. *Pharmaceuticals*. 2022;15:29. doi:10.3390/ph15010029.
- Ionescu RM, Vlasak J, Price C, Kirchmeier M. Contribution of variable domains to the stability of humanized IgG1 monoclonal antibodies. *J Pharm Sci*. 2008;97:1414–26. doi:10.1002/jps.21104.
- Feige MJ, Hendershot LM, Buchner J. How antibodies fold. *Trends Biochem Sci*. 2010;35:189–98. doi:10.1016/j.tibs.2009.11.005.
- Bertz M, Buchner J, Rief M. Mechanical Stability of the Antibody Domain CH3 Homodimer in Different Oxidation States. *J Am Chem Soc*. 2013;135:15085–91. doi:10.1021/ja405076j.
- Pedersen ME, Haegbaert RMS, Østergaard J, Jensen H. Size-based characterization of adalimumab and TNF-α interactions using flow induced dispersion analysis: assessment of avidity-stabilized

- multiple bound species. *Sci Rep.* 2021;11:4754. doi:10.1038/s41598-021-84113-z.
33. Lua WH, Ling WL, Yeo JY, Poh JJ, Lane DP, Gan SKE. The effects of Antibody Engineering CH and CL in Trastuzumab and Pertuzumab recombinant models: impact on antibody production and antigen-binding. *Sci Rep.* 2018;8:718. doi:10.1038/s41598-017-18892-9.
 34. Tan S, Liu K, Chai Y, Zhang CWH, Gao S, Gao GF, Qi J. Distinct PD-L1 binding characteristics of therapeutic monoclonal antibody durvalumab. *Protein Cell.* 2018;9:135–39. doi:10.1007/s13238-017-0412-8.
 35. Baeuerle PA, Reinhardt C. Bispecific T-cell engaging antibodies for cancer therapy. *Cancer Res.* 2009;69:4941–44. doi:10.1158/0008-5472.CAN-09-0547.
 36. Goletz C, Lischke T, Harnack U, Schiele P, Danielczyk A, Rühmann J, Goletz S. Glyco-engineered anti-human programmed death-ligand 1 antibody mediates stronger CD8 T cell activation than its normal glycosylated and non-glycosylated counterparts. *Front Immunol.* 2018;9:1614. doi:10.3389/fimmu.2018.01614.
 37. Liu Y, Lee AG, Nguyen AW, Maynard JA. An antibody Fc engineered for conditional antibody-dependent cellular cytotoxicity at the low tumor microenvironment pH. *J Biol Chem.* 2022;298:101798. doi:10.1016/j.jbc.2022.101798.
 38. Guo C, Chen F, Xiao Q, Catterall HB, Robinson JH, Wang Z, Mock M, Hubert R. Expression liabilities in a four-chain bispecific molecule. *Biotechnol Bioeng.* 2021;118:3744–59. doi:10.1002/bit.27850.
 39. Tustian AD, Endicott C, Adams B, Mattila J, Bak H. Development of purification processes for fully human bispecific antibodies based upon modification of protein a binding avidity. *Mabs.* 2016;8:828–38. doi:10.1080/19420862.2016.1160192.
 40. Gunasekaran K, Pentony M, Shen M, Garrett L, Forte C, Woodward A, Ng SB, Born T, Retter M, Manchulenko K, et al. Enhancing antibody Fc heterodimer formation through electrostatic steering effects: applications to bispecific molecules and monovalent IgG. *J Biol Chem.* 2010;285:19637–46. doi:10.1074/jbc.M110.117382.
 41. Atwell S, Ridgway JBB, Wells JA, Carter P. Stable heterodimers from remodeling the domain interface of a homodimer using a phage display library. *J Mol Biol.* 1997;270:26–35. doi:10.1006/jmbi.1997.1116.
 42. Moore GL, Bautista C, Pong E, Nguyen DHT, Jacinto J, Eivazi A, Muchhal US, Karki S, Chu SY, Lazar GA. A novel bispecific antibody format enables simultaneous bivalent and monovalent co-engagement of distinct target antigens. *Mabs.* 2011;3:546–57. doi:10.4161/mabs.3.6.18123.
 43. De Nardis C, Hendriks LJA, Poirier E, Arvinte T, Gros P, Bakker ABH, De Kruif J. A new approach for generating bispecific antibodies based on a common light chain format and the stable architecture of human immunoglobulin G1. *J Biol Chem.* 2017;292:14706–17. doi:10.1074/jbc.M117.793497.
 44. Gasteiger E, Hoogland C, Gattiker A, Duvaud S, Wilkins MR, Appel RD, Bairoch A. Protein Identification and Analysis Tools on the ExPASy Server. *Proteomics Protoc Handb.* 2005;1:571–607.